ELSEVIER

Journal of Power Sources 76 (1998) 81–90

JOURNAL OF POWER SOURCES

Electrochemical investigation of $CrO_{2.65}$ doped $LiMn_2O_4$ as a cathode material for lithium-ion batteries

D. Zhang, B.N. Popov *, R.E. White

Department of Chemical Engineering, University of South Carolina, Columbia, SC 29208, USA

Received 21 May 1998; accepted 24 July 1998

Abstract

Quaternary spinels doped with chemically modified chromium oxide ($mCrO_{2.65}$) $LiCr_yMn_{2-y}O_4$ with $y = 0.02$, 0.05 and 0.1 completely stabilize the spinel structure. Cyclic voltammograms of pure spinel exhibit high irreversibility compared with that obtained initially. The spinel doped with chemically modified chrome oxide $mCrO_{2.65}$ causes the peak separation to decrease contributing to the electrochemical reversibility of the doped cathode material. Negligible shift of the peak potentials was observed for these cathodes. Chromium dopant enhances the mass transfer of Li^+ in the active material. The Li^+ diffusion coefficient in $LiCr_{0.1}Mn_{1.9}O_4$ estimated from an analysis of the Warburg impedance is two order of magnitude higher than that in pure spinel.

Keywords: Chemically modified chromium oxide; Doped spinel; Capacity retention; Electrochemical impedance spectroscopy

1. Introduction

Spinel lithium manganese oxide attracted interest among researchers because of its economical and environmental advantages compared to other lithiated transition metal oxides such as lithium cobalt oxide or lithium nickel oxide [1–15]. However, efforts to substitute $LiMn_2O_4$ for $LiCoO_2$ in commercial Li-ion batteries have not been successful due to the rapid capacity fade upon cycling [16]. This capacity fading has been suggested to be due to spinel dissolution [16], the Jahn–Teller effect [17], and lattice instability [18].

Gummow et al. [17] and Tarascon et al. [12] attempted to optimize the lithium manganese oxide cathode by adding extra lithium in the active spinel material. Unfortunately, the capacity fade of these cathodes was still high and the capacity dropped to 80% of the initial discharge capacity (100 mA h/g, based on the mass of cathode) after 300 cycles at C/2 rate. This capacity fade was attributed to the irreversible loss of the capacity of the spinel cathode upon cycling [10].

Quaternary spinels of the general formula $LiM_yMn_{2-y}O_4$ (M = Cr, Co, Ni) were able to alleviate the capacity fade of the cathode upon cycling [19–24]. According to Guohua et al. [19], $LiM_yMn_{2-y}O_4$ (M = Co, Cr, and Ni) showed improved cycle life at the expense of capacity. Recently, Sigala et al. [20] reported that a chromium substitution (Cr_2O_3) was beneficial to the specific capacity and energy of the spinel.

Low levels of trivalent cations were used by Robertson et al. [23,24] to stabilize spinel $LiMn_2O_4$ cathode material. It was found that only $LiCr_{0.02}Mn_{1.98}O_4$ exhibited acceptable initial reversible capacity. The optimum composition in their electrochemical stabilization studies with Cr^{3+} had a discharge capacity of 110 mA h/g after 100 cycles at 0.5 mA/cm^2. Capacity losses in 4 V $LiMn_2O_4$ based spinel systems were attributed to Mn dissolution into the electrolyte causing structural degradation of the cathode.

In this work an attempt was made to stabilize the spinel structure by modifying the oxygen stoichiometry, the manganese valent state and the lattice constants using $mCrO_{2.65}$ [chemically modified chromium (V–VI) oxide] [25] as a precursor. A range of $y = 0$ to $y = 0.1$ of $mCrO_{2.65}$ doped spinels ($LiCr_yMn_{2-y}O_4$) were synthesized and electrochemically characterized. The results were compared with those obtained for stoichiometric pure spinel $LiMn_2O_4$.

Electrochemical impedance spectroscopy (EIS) and linear polarization resistance techniques (LP) were used to determine the transport and the electrochemical kinetic parameters of the above active materials. The capacity fade

* Corresponding author. Tel.: +1-803-777-7314; Fax: +1-803-777-8265; E-mail: bnp@sun.che.sc.edu

0378-7753/98/$19.00
PII: S0378-7753(98)00143-8

of all cathode materials was studied and the active materials loss during cycling was determined. Also the effect of Cr content in the spinel on its self discharge was investigated.

2. Experimental

Crystalline CrO_x was prepared by heating CrO_3 in an autoclave for 24 h at 260°C under oxygen pressure of 1000 psi. The product was a mixture between CrO_x and residual CrO_3. The CrO_3 impurity was removed by leaching the product in water for 1 h and by chemically treating the product which modifies the dispersive state of the cathode material and completely removes the traces of CrO_3 contamination. Thermogravimetric analysis (TGA) was carried out on CrO_x samples in air at 1°C/min to determine the O/Cr ratio. The O/Cr ratio in chemically modified CrO_x ($mCrO_x$) prepared at 260° and pressure of 1000 psi was 2.65. Chemically modified $mCrO_{2.65}$ has different properties than CrO_3. It is neither hydroscopic nor soluble in water and thus is not a biohazard.

The $mCrO_x$ doped $LiCr_yMn_{2-y}O_4$ compounds (y = 0.02, 0.05, 0.1) were synthesized by solid state reaction. A stoichiometric mixture between Li_2CO_3 (Aldrich, 99.9%), Mn_2O_3 (Aldrich, 99.9%) and $mCrO_{2.65}$ was preheated in autoclave at 600°C and oxygen pressure of 500 psi for 15 h and then heated at 650°C for two days with intermittent grounding, followed by slow cooling (about 2°C min^{-1}).

A roller-pressed, round thin film cathode was prepared from active powder material, carbon black and polytetrafluoroethylene (PTFE) binder in a weight ratio 1:0.1:0.05. Electrochemical characterization of the cathode materials was carried out using a Swagelock three electrode cell. The anode and the reference electrodes were discs of lithium foil, and a sheet of Whatman glass fiber membrane acted as the separator.

The electrolyte contained 1 M LiPF6 dissolved in a mixture of ethylene carbonate (EC), dimethyl carbonate (DMC), and diethyl carbonate (DEC) in a ratio 4:4:3. The T-cell was assembled carefully in a glovebox filled with argon. The cathode had a diameter of 1.25 cm (an area of 1.23 cm^2) and a thickness of 50 μm with a total mass of 16.0 mg. It was heated in a mini-furnace at 300 C for 1 h in the glovebox before assembling. The cathode and anode separation was approximately 0.3 mm. After the cell was assembled, it was left in the glovebox for half an hour enabling the electrolyte to disperse into the porous structure of the cathode before cycling and other electrochemical characterization. Charge/discharge curves were obtained galvanostatically using current densities of 0.1 mA/cm^2 (C/14) or 0.7 mA/cm^2 (C/2). The cells were tested on Arbin cycler with cut-off potentials of 3.4 and 4.4 V.

EIS experiments were carried out at different states of charge on ternary spinel and $mCrO_{2.65}$ doped spinel. The impedance covered the frequency range from 0.002 Hz to 100 kHz with an 'ac' voltage signal of 5 mV. The Cr doped spinels were characterized by X-ray diffraction using a Rigaku 405S5 diffractometer with Cu Kα radiation. The specific surface area of the material was measured using a Micromeritics Pulse Chemisorb 2700, according to the Brunauer–Emmett–Teller (BET) single point method with nitrogen physiosorption. The samples were dried for 1 h under argon flow at 200°C before the BET measurements. Cyclic voltammograms were obtained using a scan rate 0.1 mV/s over a potential range of 3.4 to 4.4 V vs. Li/Li^+ reference electrode.

3. Results and discussion

The powder XRD patterns of the $mCrO_{2.65}$ doped spinel $LiCr_yMn_{2-y}O_4$ with $y = 0$, 0.02, 0.05 were identified as single-phase spinel. The results indicated that when the $mCrO_{2.65}$ is doped into $LiMn_2O_4$, the structure of the ternary spinel remains while some of the manganese atoms in the spinel phase are replaced by chromium atoms. Similar results were reported in literature for Cr^{3+} doped spinel. According to Mosbach et al. [26], Thackeray et al. [2,27] and David et al. [28], the lattice parameters of $LiCr_yMn_{2-y}O_4$ were very close to those of $LiMn_2O_4$ and both compounds belong to the same space group (Fd3m) in which Mn-ions are at 16d sites while the O-ions are at 32 e sites. Also Pistoia et al. [29] and Guohua et al. [19] found that Cr-doped spinels have cubic structure. X-ray diffraction data of $LiCr_yMn_{2-y}O_4$ (y = 0, 0.2, 0.4 and 0.6) by Baochens et al. [22] indicated a cubic spinel with $\sum|d_{obs} - d_{cal}|/\sum d_{obs} = 4.4 \times 10^{-4}$ for more than 40 observations.

Assuming an ideal cubic spinel structure, the lattice parameters for each sample are given in Table 1. The average Mn–Mn and Mn–O interatomic distances were calculated using the equation $R_{Mn-Mn} = a\sqrt{2}/4$ and $R_{Mn-O} = a(3u^2 - 2u + 0.375)^{0.5}$, respectively. The constant $u = 0.265$ is the oxygen positional parameter [3].

The lattice parameters shown in Table 1 decreased only initially when the $mCrO_x$ was doped into the spinel under high pressure. The estimated lattice values for $y = 0$, 0.02, 0.05 and 0.1 in $LiCr_yMn_{2-y}O_4$ were 8.221, 8.214, 8.218

Table 1
Unit cell parameters and interatomic distance for $LiCr_yMn_{2-y}O_4$ from $CrO_{2.65}$ precursor

$LiCr_yMn_{2-y}O_4$	a (Å)	V (Å^3)	$R_{Mn-Mn(Cr)}$ (Å)	$R_{Mn(Cr)-O}$ (Å)
$y = 0$	8.221(1)	555.6(2)	2.906	1.940
$y = 0.02$	8.214(1)	554.2(2)	2.904	1.938
$y = 0.05$	8.218(1)	555.0(2)	2.905	1.939
$y = 0.1$	8.215(1)	554.5(2)	2.904	1.937

and 8.215 A, respectively indicating a departure from the Vegard's law [30]. According to the Vegard's Law, the unit cell parameters should change linearly with the change of the composition. The unit cell data presented in Table 1 for CrO_x doped spinel showed a negative departure from linearity at $y = 0.02$. The results can be explained taking into account the following: Vegard's law assumes that the change in the unit cell parameters with composition depends on the relative sizes of the 'active' atoms or ions in the solid solution mechanism and that the ions replace each other in a simple substitution mechanism which is generally not a case in the real systems. In fact, departure from Vegard's law behavior has been reported in the literature. Both positive and negative departures from ideality were observed [31]. Larger changes of unit cell volume or discontinuity may occur at certain compositions if either a change in symmetry or a change in the solid solution mechanism occurs. Example of the latter is provided by a (partial) range of solid solutions between Li_4SiO_4 and Zn_2SiO_4 [32]. A negative departure from Vegard's Law was also observed by Tena et al. [33]. They attempted to prepare orthorhombic phase of $Fe_{0.4}Ti_{0.2-x}Sn_xNb_{0.4}O_2$ $(0 \le x \le 0.2)$ by colloidal methods. According to these authors the unit cell volume of the orthorhombic phase undergoes a large drop with a small addition of Sn-ions at $x = 0.05$. The same phenomena was observed by Greatrex et al. [34] and Shimony and Ben-Dor [35].

In the same oxidation state, chromium ions have smaller radius than manganese ions [36]. For example, the radius of Mn^{3+} ion is 0.68 Å, while the ionic radius of Cr^{3+} is 0.615 Å. According to Vegard's law the Cr-substituted spinel should have smaller lattice parameters than pure spinel regardless of the relative cation concentration. Substitution of Cr^{3+} or Cr^{4+} (0.58 Å) for Mn^{3+} or Mn^{4+} (0.60 Å) will result in shrinkage of unit cell volume which increases the stability of the structure during lithium intercalation/deintercalation reactions. Also, the unit cell volume should decrease linearly with increase of the Cr content in the spinel. The observed negative departure from the Vegard's law of the unit cell parameters in Table 1 are probably due to a short distances cation ordering which occurs in the vicinity of $y = 0.02$.

The estimated values of unit cell volume for $LiCr_{0.02}Mn_{1.98}O_4$, $LiCr_{0.05}Mn_{1.95}O_4$ and $LiCr_{0.1}Mn_{1.9}O_4$ are 554.2, 555.0, and 554.5 Å^3, respectively. The $Li_xCr_yMn_{2-y}O_4$ volume changes during cycling for $y = 0$ ($V = 561.31$ Å^3 for a fully intercalated, and $V = 520.69$ Å^3 for a fully deintercalated spinel) and for $y = 0.1$ ($V = 554.5$ Å^3 for a fully intercalated and $V = 520.6$ Å^3 for a fully deintercalated spinel) were 7.2% and 6.1%, respectively. The stability of the structure increases with the decrease of the volume shrinkage [19–21]. The improvement of the cycle performance of $mCrO_{2.65}$ doped spinel as in the case of Co doped spinel was attributed to the stabilization of the spinel structure [21]. Also, the binding energy of MnO_2 (α type) and CrO_2 are 946 and 1142 kJ/mol, respectively [19]. The stronger CrO_2 bond contributes to the overall stabilization of the octahedral sites.

The specific surface area was measured using a Micromeritics Pulse Chemisorb 2700, according to the Brunauer–Emmett–Teller (BET) single point method with nitrogen physiosorption. The samples were previously dried 1 h under argon flow at 200°C. The BET surface area of $mCrO_x$ doped spinel at 650°C and oxygen pressure of 500 psi with $y = 0$, 0.02; 0.05 and 0.1 were 2.9, 2.7, 2.8 and 2.6 m^2/g. The results indicated that the surface area of temperature and pressure treated spinels does not change significantly when doped with $mCrO_{2.65}$. Note that there is a significant change of the average surface area from 3.2 to 2.9 cm^2/g when spinel is treated at high temperature and oxygen pressure of 500 psi.

Fig. 1a and b show the galvanostatic charge-discharge profiles obtained for pure spinel and $mCrO_{2.65}$ doped spinel ($LiCr_{0.1}Mn_{1.9}O_4$). For the pure spinel two distinct plateaus, which are characteristic of a reversible two-stage process of $LiMn_2O_4$ structure, were observed during charging and discharging the electrode [8–10]. The plateaus tend to merge into one plateau with an increase of the number of cycles. A large capacity loss was observed in Fig. 1a when cycling undoped spinel compared with the $mCrO_{2.65}$ doped spinel (Fig. 1b). The $mCrO_{2.65}$ improves the cycling performance and completely stabilizes the spinel.

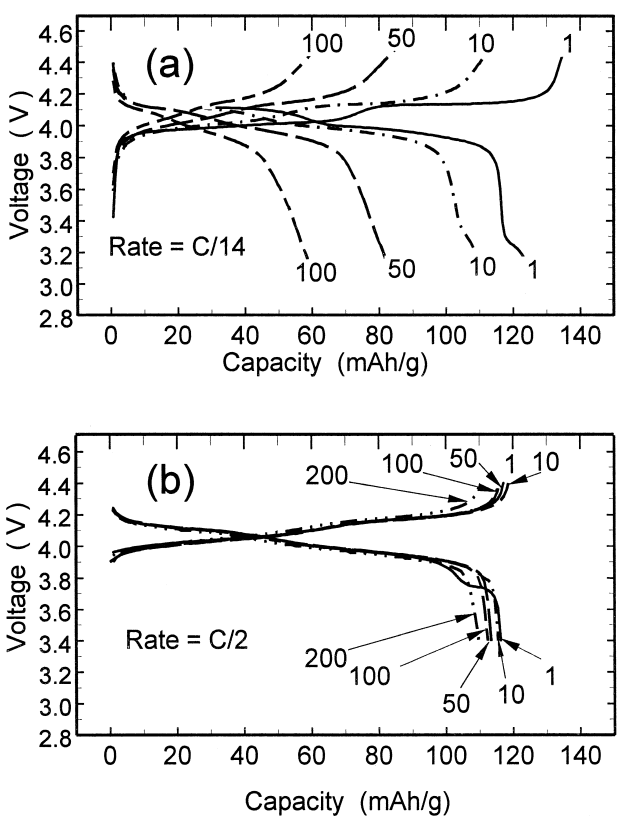

Fig. 1. Galvanostatic charge–discharge curves of (a) $LiMn_2O_4$ and (b) $LiCr_{0.1}Mn_{1.9}O_4$.

Cr^{3+} ions are formed during synthesis of $LiCr_yMn_{2-y}O_4$ by reduction of $CrO_{2.65}$ at 600°C. These ions fit the $LiMn_2O_4$ lattice since Cr^{3+} has a very stable d^3 configuration, it is not easily oxidized, prefers octahedral sites and exhibits the proper ionic radius of 0.615 Å. As found by Robertson et al. [23,24], the ionic radius of the dopant and its preference for octahedral coordination are critical factors in the electrochemical stability of $LiMn_2O_4$.

Fig. 2 shows typical galvanostatic charge-discharge cycling performance curves for electrodes cycled at C/14 rate made from pure spinel. The $mCrO_{2.65}$ doped spinel cathodes, $LiCr_yMn_{2-y}O_4$ (with $y = 0.02$ 0.05, and 0.1) were cycled at C/2 rate since they showed in the preliminary experiments very good cycling performance at high discharge rates.

As shown in Fig. 2, $mCrO_{2.65}$ doped spinel $LiCr_{0.1}Mn_{1.9}O_4$ showed the best cycle performance. Even using a seven times higher discharge rate (0.7 mA/cm^2 or C/2) than that for the pure spinel, the capacity of $mCrO_x$ doped spinel remains almost the same after 200 cycles as the initial capacity.

Fig. 3 compares the initial CV curve obtained for pure spinel and CV curve obtained for $mCrO_{2.65}$ doped spinel ($LiCr_{0.02}Mn_{1.98}O_4$). As shown in this figure, the small amount of dopant causes the anodic/cathodic peak separation to decrease thus improving the electrochemical reversibility of the doped cathode material.

Fig. 4 shows the initial cyclic voltammograms and those obtained after the 100th cycle of pure spinel and $mCrO_{2.65}$ doped spinel, $LiCr_yMn_{2-y}O_4$ with $y = 0.02$, 0.05 and 0.1. The experiments were performed using a sweep rate of 0.1 mV/s. As shown in Fig. 4a, after 100 charge–discharge cycles, the pure spinel cyclic voltammogram exhibits high irreversibility when compared with the cyclic voltammogram obtained initially. The anodic peak shifts approximately 0.26 V in anodic direction, while the cathodic peak shifts 0.12 V in cathodic direction when compared to the initial values. Also, the peak currents drop to half of those observed in the first cycle. The observed shift of the peak potential contributes to the increased instability of the electrolyte, which results in higher capacity fade of pure spinel. It is obvious from Fig. 4b–d that $mCrO_{2.65}$ doped spinel, $LiCr_yMn_{2-y}O_4$ cathodes with $y =$ 0.02, 0.05 and 0.1 are completely stabilized. Negligible shift of the peak potential and consequently negligible reduction of the initial capacity was observed for these cathodes.

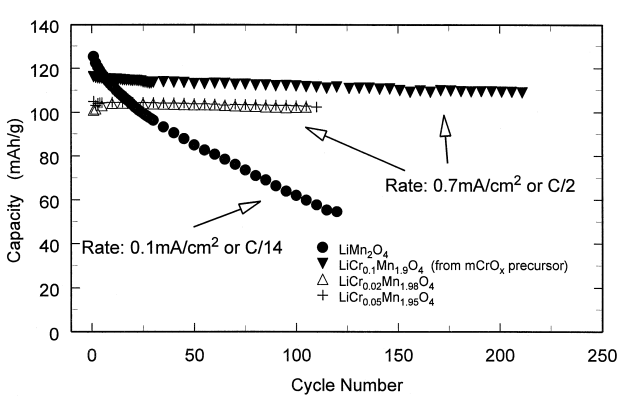

Fig. 2. Cycling performance of different cathode materials.

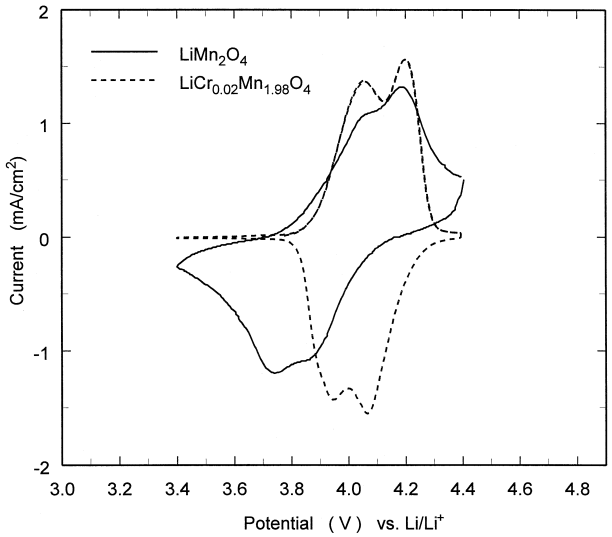

Fig. 3. Comparison of the initial cyclic voltammograms of $LiMn_2O_4$ and $LiCr_{0.1}Mn_{1.9}O_4$ at 0.1 mV/s scan rate.

3.1. Determination of electrochemical kinetic parameters for pure and $mCrO_x$ doped spinels

Electrochemical Impedance Spectroscopy (EIS) and the linear polarization technique (LP) were used to determine the total resistance (R_t), charge transfer resistance (R_{ct}), surface layer resistance (R_{sl}), and exchange current density of pure and $mCrO_x$ doped spinels at various states of charge. The experimental procedure was described previously [21,37,38]. The electrode was charged galvanostatically to a fully charged state (4.4 V vs. Li/Li$^+$). Next, linear polarization and electrochemical impedance spectroscopy experiments were carried out. Then the electrode was discharged for a certain period of time and the same measurements were conducted. The procedure was repeated until the electrode was discharged to the cut-off potential of 3.3 V.

The total resistance determined using the linear polarization technique is equal to the charge transfer resistance only when the charge transfer step dominates the electrode process and the ohmic resistance of the electrode system is negligible [37,38]. In such a case, at low overpotentials, linearization of the Butler–Volmer equation [39]

$$i = i_0\left\{\exp\left(\frac{(1-\beta)F\eta}{RT}\right) - \exp\left(-\frac{\beta F\eta}{RT}\right)\right\} \quad (1)$$

results in

$$R_{ct} = \frac{RT}{Fi_0} = \frac{\eta}{i} \text{ with } i_0 = AnFkc^{1-\beta}(c_t - c_s)^{1-\beta}(c_s)^{\beta} \quad (2)$$

where i_o is the exchange current density, β is symmetry factor, η is overpotential, k is the reaction rate constant, c is concentration of electrolyte in the liquid phase, c_t is the concentration of total site in the solid host material available for insertion of lithium ions, and c_s is the concentration of lithium ions in the solid phase. When the ohmic resistance is not negligible, Eq. (2) can be used to estimate the sum of the ohmic resistance and the charge transfer resistance, which causes the exchange current density to be underestimated. This limitation of LP method can be overcome by using EIS, which provides an estimation of the exchange current density without the interference of the ohmic resistance.

EIS experiments were carried out on both pure spinel and $mCrO_{2.65}$ doped spinel $LiCr_{0.1}Mn_{1.9}O_4$. The impedance data covered the frequency range from 0.002 Hz to 100 kHz with an 'ac' voltage of 5 mV. The Nyquist plots obtained initially for pure spinel and $mCrO_x$ doped spinel cathodes ($Li_{0.3}Cr_{0.1}Mn_{1.9}O_4$) and those obtained after 25, 50 and 100 cycles are presented in Fig. 5a–d. For both the pure spinel and $mCrO_{2.65}$ spinel, a depressed semicircle or two semicircles were observed. The equivalent circuit is based on assumptions that the electrode consists of a rough but continuous interconnected, porous solid of low bulk resistance. The faradic contribution at low frequency is represented by a charge transfer resistance R_{ct} and by Warburg impedance Z_W, which includes a diffusion-controlled process in the solid. At low frequencies, uniform charging of the electrode results in the formation of double layer capacitance C_{dl}. The electrolyte resistance is presented by R_s.

R_{sl} in the equivalent circuit presented in Fig. 5a represents the ion transfer resistance and C_{sl} is the capacitance of the surface layer. To account for the depression of the semicircle (i.e., the shift of the center of the circle to the position below the abscissa), a Constant Phase Element (CPE) in series with the double-layer capacitance (C_{dl}) was introduced into the model [40]. The component values of the equivalent circuit shown in Fig. 5 were obtained by fitting the ac impedance data using Solatron® impedance graphing and analysis software Zview™ (Scribner Associates).

Fig. 6 shows the charge transfer resistance values obtained from EIS as a function of cycle number compared with those obtained with a linear polarization technique. The charge transfer resistance values for pure spinel ($y = 0$) were higher than those estimated for $mCrO_x$ doped spinel with optimized $mCrO_x$ content of $y = 0.1$. The average

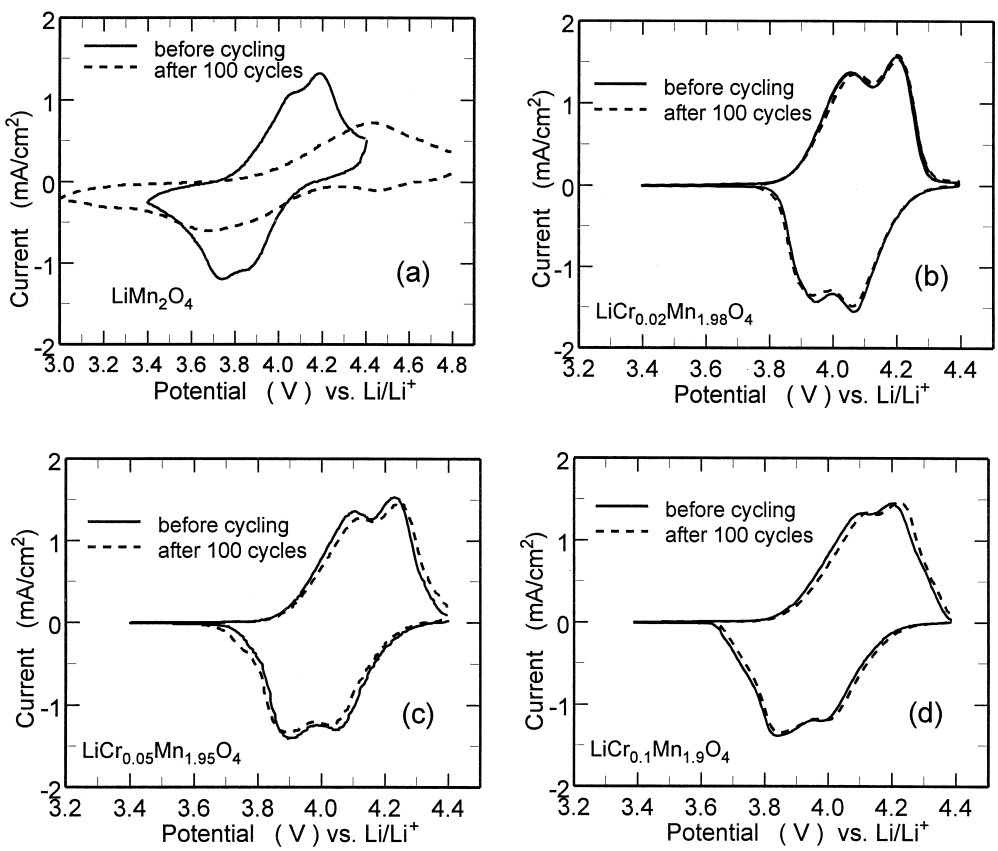

Fig. 4. Cyclic voltammograms of (a) $LiMn_2O_4$, (b) $LiCr_{0.02}Mn_{1.98}O_4$, (c) $LiCr_{0.05}Mn_{1.95}O_4$, and (d) $LiCr_{0.1}Mn_{1.9}O_4$ cathode.

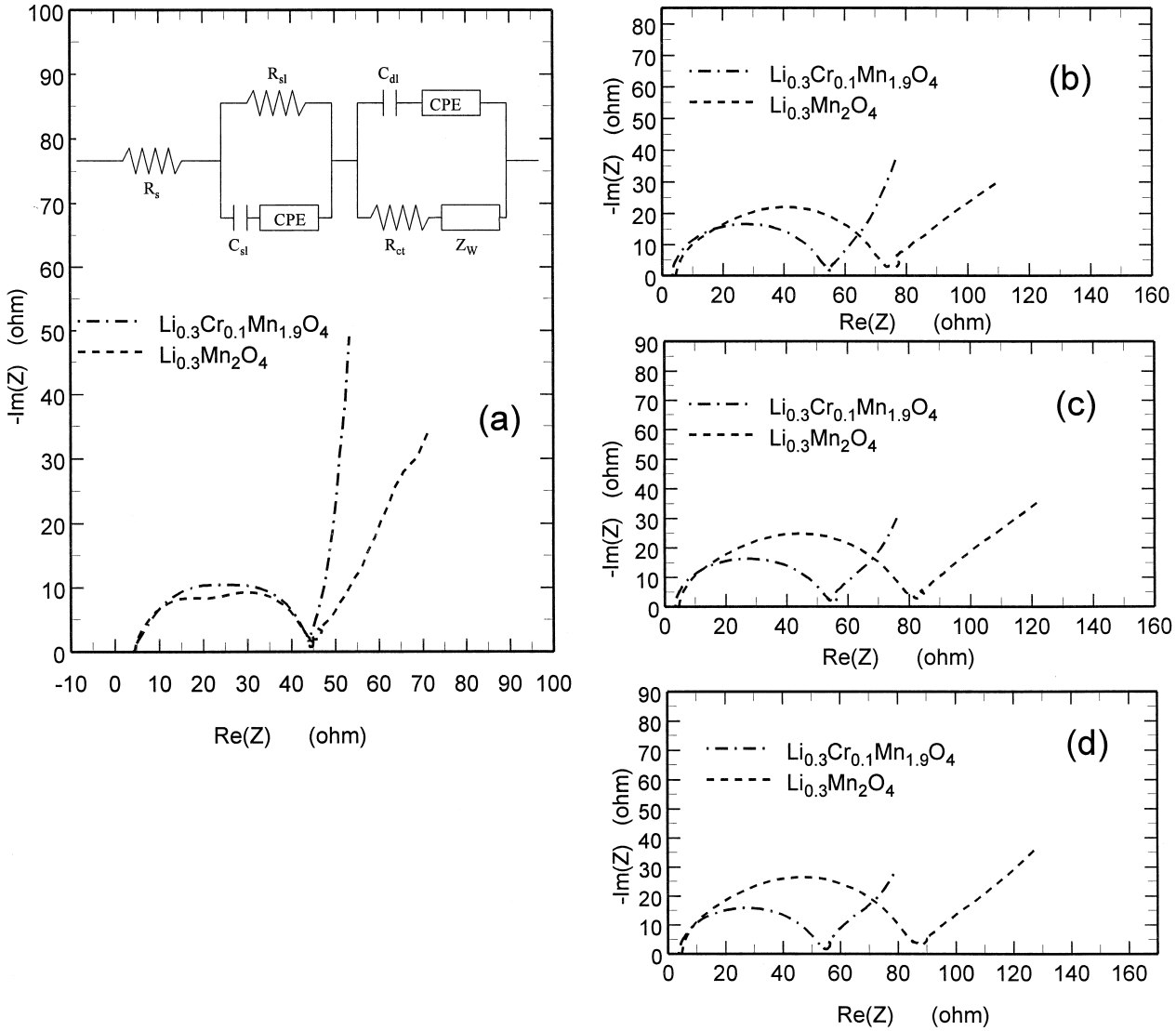

Fig. 5. Nyquist plots of $Li_{0.3}Mn_2O_4$ and $Li_{0.3}Cr_{0.1}Mn_{1.9}O_4$ cathodes obtained at C rate. (a) After first cycle, (b) after 25 cycles, (c) after 50 cycles, and (d) after 100 cycles.

charge transfer resistance values estimated for pure and $mCrO_x$ doped spinel for different cycle numbers were 0.505 Ω g and 0.410 Ω g, respectively. The presence of $mCrO_x$ decreases a small amount of the charge transfer resistance and facilitates the charge transfer reaction.

The exchange current densities for pure and $mCrO_x$ doped spinel were estimated using Eq. (2). The results are presented in Fig. 7 as a function of cycle number. The charge transfer resistances used to calculate the exchange current densities were estimated by fitting the AC-impedance data. The average exchange current densities of $mCrO_x$ ($y = 0.1$) doped and pure spinels are 61.6 mA/g and 51.2 mA/g, respectively. The surface area of pure spinel determined by BET was 3.20 m^2/g, giving an exchange current density of 1.60×10^{-6} A/cm^2 for the pure spinel, which is in agreement with a literature reported value of 1.30×10^{-6} A/cm^2 in a similar case [40]. The surface area of $mCrO_x$ doped spinel determined by BET was 2.60 m^2/g, which gives an exchange current density of 1.93×10^{-6} A/cm^2.

Fig. 8 shows the surface layer resistance as a function of cycle number for pure spinel and for $mCrO_x$ doped spinel $Li_{0.3}Cr_{0.1}Mn_{1.9}O_4$. The observed increase of the resistance in Fig. 8 is due to the slow growth of the passive film as a function of time. For pure spinel, the rate of growth of the surface layer was rapid in the initial 40 h (twenty cycles) and, thereafter, the film grows slowly. The surface layer resistance estimated 1.5 h after the construction of the cell (0 cycles) was 0.069 Ω g (5.51 Ω). After 50 cycles (100 h), the R_{sl} increases to 0.48 Ω g (38.5 Ω). From 50 to 100 cycles (200 h after the construction of the cell), the film resistance grows slowly to 0.51 Ω g. Similar results were obtained by Thomas et al. [41] who reported from their impedance analysis of polycrystalline Li_{1-x}-

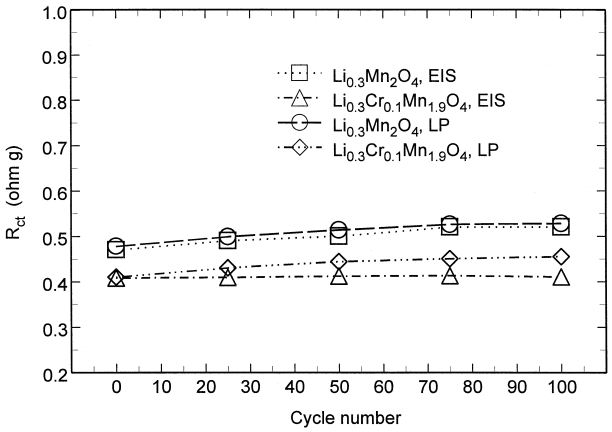

Fig. 6. Charge transfer resistance (R_{ct}) evaluated from Linear Polarization (LP) and Electrochemical Impedance Spectroscopy (EIS) as a function of cycle number for $Li_{0.3}Mn_2O_4$ and $Li_{0.3}Cr_{0.1}Mn_{1.9}O_4$ cathodes.

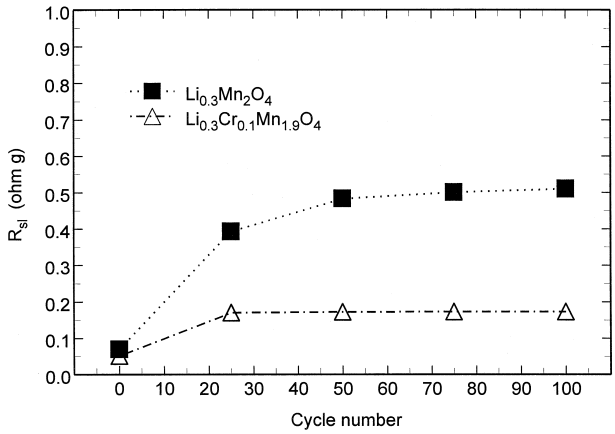

Fig. 8. The surface layer resistance as a function of cycle number (at C rate) for $Li_{0.3}Mn_2O_4$ and $Li_{0.3}Cr_{0.1}Mn_{1.9}O_4$ cathodes.

CoO_2 that the rate of growth of the surface layer was rapid over the first 6 h after the construction of the cell.

As shown in Fig. 8, the $mCrO_x$ doped spinel form a passive film which has lower resistance than undoped material. The surface layer resistance estimated 1.5 h after the construction of the cell (0 cycles) was estimated to be 0.051 Ω g (4.02 Ω). The rate of increase of the surface layer resistance of $mCrO_x$ doped spinel is small. It was found that at 25th cycle (50 h), the surface layer resistance increases only to 0.17 Ω g (13.4 Ω) and the curve levels off thereafter.

Fig. 9 shows the dependence of C_{dl} and C_{sl} values for pure spinel as a function of cycle number. The values of the C_{dl} estimated for the pure spinel and for the $mCrO_{2.65}$ doped spinel at 25th cycle are 26.5 μF and 27.4 μF, respectively. The results indicated that the effective surface are of the electrode and, consequently, the double layer capacitance do not increase with time due to the complete flooding of the electrode.

The dependence of the surface layer capacitance for both the pure spinel and $mCrO_x$ doped spinel on cycle number is also presented in Fig. 9. Since $C_{sl} = S/l$, the surface layer capacitance should decrease with the increase of the surface layer thickness l (surface layer resistance R_{sl}). As shown in Fig. 9, the initial surface layer capacitance of pure spinel is 27 μF. After 25 cycles or 50 h after the construction of the cell, the surface layer capacitance decreases to a value of 14.1 μF. The observed decrease of the surface layer capacitance is in agreement with the estimated increase of the surface layer resistance in Fig. 8.

The initial surface layer capacitance of $Li_{0.3}Cr_{0.1}Mn_{1.9}O_4$ is 29.7 μF and slowly decreases to a value of 26.1 μF after 100 cycles. The results are in agreement with the observed small increase of the surface layer resistance $Li_{0.3}Cr_{0.1}Mn_{1.9}O_4$ in Fig. 8.

The Nyquist plots obtained after 100 cycles for completely discharged pure spinel $Li_{0.9}Mn_2O_4$ and for $mCrO_x$ doped spinel $Li_{0.9}Cr_{0.1}Mn_{1.9}O_4$ are shown in Fig. 10. The charge transfer resistance of $Li_xMn_2O_4$ shows a significant increase with a decrease of the state of charge. The charge transfer resistance of $Li_{0.9}Mn_2O_4$ (1.06 Ω g) obtained by fitting the data obtained from Fig. 10 increases more than two times from the value estimated for

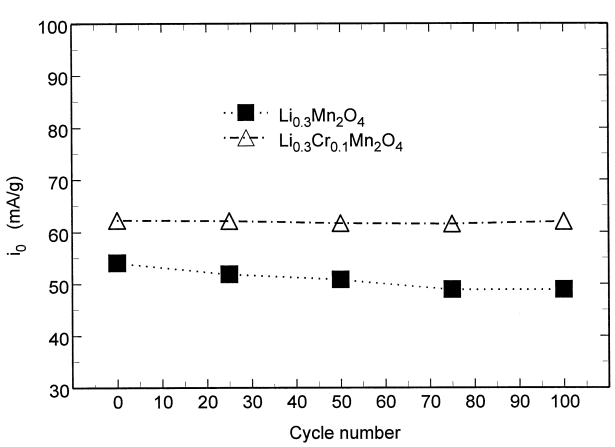

Fig. 7. Exchange current density as a function of cycle number for $Li_{0.3}Mn_2O_4$ and $Li_{0.3}Cr_{0.1}Mn_{1.9}O_4$ cathodes.

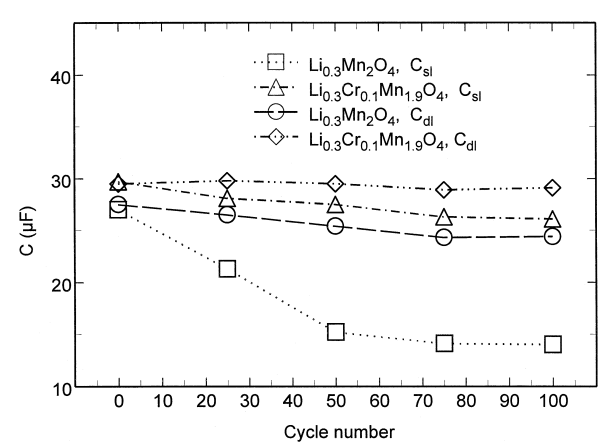

Fig. 9. Interfacial capacitance as a function of cycle number (at C rate) for $Li_{0.3}Mn_2O_4$ and $Li_{0.3}Cr_{0.1}Mn_{1.9}O_4$ cathodes.

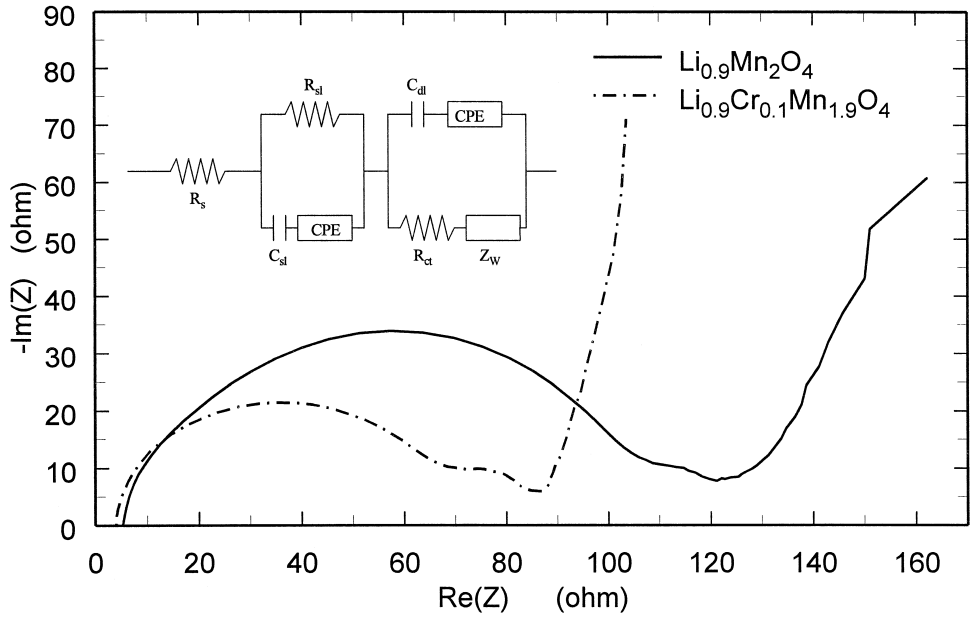

Fig. 10. Comparison of Nyquist plots of $Li_{0.9}Cr_{0.1}Mn_{1.9}O_4$ and $Li_{0.9}Mn_2O_4$ cathodes after 100 cycles at C rate.

$Li_{0.3}Mn_2O_4$ in Fig. 6. The charge transfer reaction occurs much more easily on $Li_{0.3}Mn_2O_4$ than on $Li_{0.9}Mn_2O_4$.

Similar results were obtained for $mCrO_x$ doped spinel. The charge transfer resistances estimated for $Li_{0.9}Cr_{0.1}Mn_{1.9}O_4$ and $Li_{0.3}Cr_{0.1}Mn_{1.9}O_4$ were 0.778 Ω g and 0.410 Ω g, respectively.

3.2. Determination of lithium-ion diffusion coefficient in the spinels

The Li^+ ion diffusion coefficient can be obtained from an analysis of the Warburg impedance [40,42]

$$\mathrm{Re}(Z_W) = B\omega^{-1/2} \text{ and } -\mathrm{Im}(Z_W) = B\omega^{-1/2} \quad (3)$$

where ω is the angular frequency, and B is the Warburg coefficient. The numerical value of the Li^+ diffusion coefficient in the cathode can be estimated from Eq. (4) when $\gg 2D_{Li+}/L^2$.

$$D_{Li^+} = 0.5\left[\frac{V_m}{FSB}\left(-\frac{dE}{dx}\right)\right]^2 \quad (4)$$

where L is the finite length of the diffusion process, V_m is molar volume of the spinel material (42.25 cm^3/mol for $LiMn_2O_4$), S is the apparent surface area of the electrode, and $(dE)/(dx)$ is the slope of the open-circuit potential vs. mobile ion concentration x at each x value. The Warburg coefficient was obtained from the slope of $\mathrm{Re}(Z)$ vs. $\omega^{-1/2}$ or $-\mathrm{Im}(Z)$ vs. $\omega^{-1/2}$.

As shown in Fig. 11, for pure spinel, $y = 0$, the D_{Li+} is in the range between 9.65×10^{-10} and 5.78×10^{-10} cm^2/s, which is in agreement with the diffusion coefficient reported in the literature [40].

For $mCrO_x$ doped spinel $Li_{0.3}Cr_{0.1}Mn_{1.9}O_4$, the Li^+ diffusion coefficient was estimated to be in the range between 3.92×10^{-8} and $7.42 \times ^{-8}$ cm^2/s which are two order of magnitude higher than those estimated for pure spinel.

3.3. Self-discharge studies

According to Pistoia et al. [43] and Guyomard and Tarascon [10], the self discharge of $LiMn_2O_4$, $LiCoO_2$ and $LiNiO_2$ electrodes is up to 6–12% in the first month. The capacity loss was found to depend upon the nature and purity of the electrolyte, temperature, storage time and upon the procedures applied to cathode and cell preparation. Self-discharge losses can be both reversible and

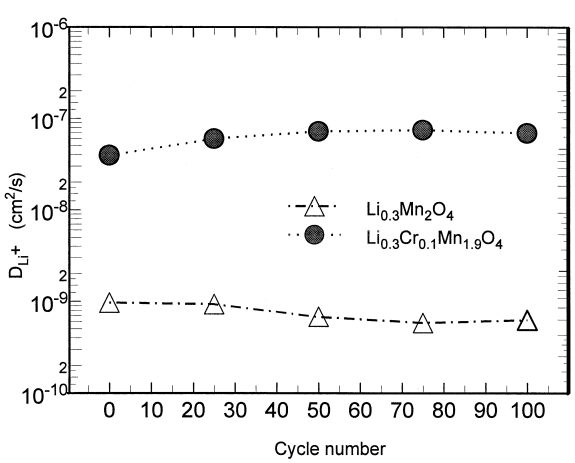

Fig. 11. Chemical diffusion coefficient of Li^+, D_{Li+}, as a function of cycle number for $Li_{0.3}Mn_2O_4$ and $Li_{0.3}Cr_{0.1}Mn_{1.9}O_4$ cathodes.

irreversible. The irreversible loss is not recoverable and contributes to the overall capacity fade of the cell.

Potentiostatic experiments were carried out in order to determine the cumulative capacity loss of pure spinel and $mCrO_{2.65}$ doped spinel. Initially, the electrode was charged to 4.3 V galvanostatically at 0.1 A/cm^2. Next, potentiostatically the potential was kept constant at 4.3 V vs. Li/Li^+ reference electrode and the floating current which counterbalances the self discharge was measured as a function of time. The floating currents and the cumulative capacity loss for a pure spinel, and $mCrO_{2.65}$ doped spinel are presented in Fig. 12. As shown in Fig. 12, the initial current drops at a relatively fast rate from the initial charging current (0.1 A/cm^2). During the initial period (10 h), the current in Fig. 12 consists of charging current under potentiostatic conditions that immediately follows the galvanostatic mode. Since the diffusion process of lithium ions in the solid phase is the rate-determining step (rds), the lithium deintercalation in the structure of the cathode has not been completed during the galvanostatic charging process and continues to occur under a potentiostatic condition until the deintercalation of lithium ion is complete. Thus, the current during the initial period of potentiostatic mode is different in nature from the current of long times which is a direct measurement of the electrolyte oxidation. In other words the self discharge current should be estimated from the floating current that results from the electrolyte oxidation. Based on this analysis, the floating current was fitted with long times as experimental equations as presented in Fig. 12. As shown in Fig. 13, the

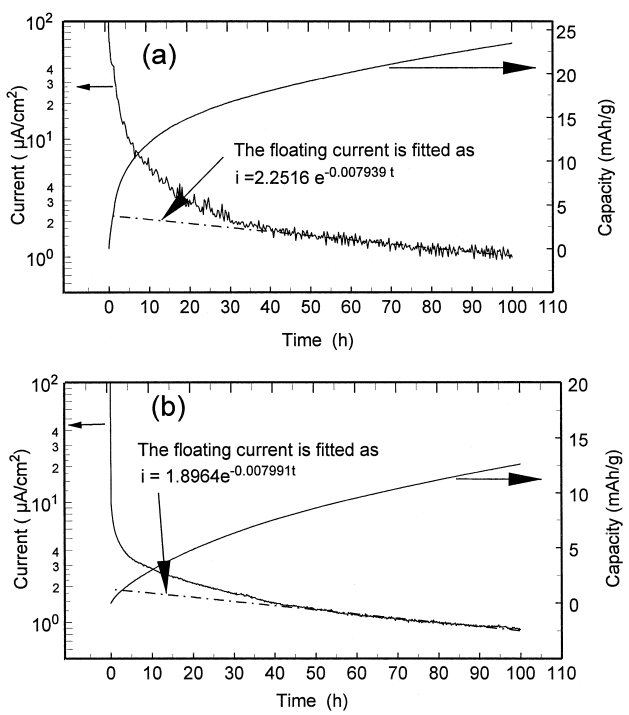

Fig. 12. Cumulative capacity (ordinate right) and floating current density (ordinate left) for (a) $LiMn_2O_4$ (b) $LiCr_{0.1}Mn_{1.9}O_4$ cathodes.

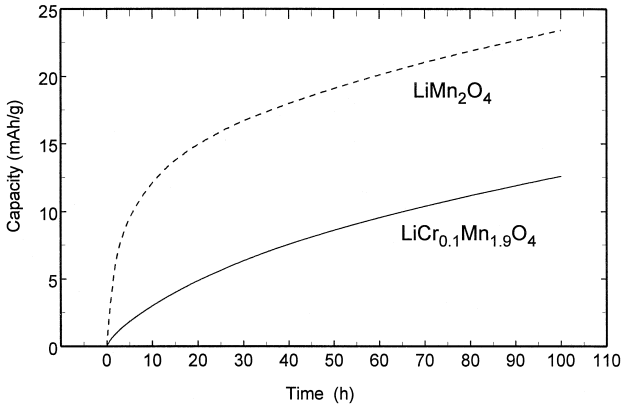

Fig. 13. Comparison of cumulative capacity.

cumulative capacity loss during 100 h estimated for pure spinel, and $mCrO_{2.65}$ doped spinel are 23.4 and 12.6 mA h/g, respectively. The results indicated that $mCrO_{2.65}$ doped spinel stabilizes the spinel structure and inhibits the passivation process at the interface that results from the electrolyte decomposition.

4. Conclusion

Chemically-modified-$CrO_{2.65}$ doped spinel, $LiCr_{0.1}Mn_{1.9}O_4$, showed the best cycle performance. The improvement of the cycle performance was attributed to the stabilization of the spinel structure. The stronger CrO_2 bond contributed to the overall stabilization of the octahedral sites. The observed decrease of the volume shrinkage of $Li_{0.3}Cr_{0.1}Mn_{1.9}O_4$ contributes to the stability of the spinel structure. $LiCr_{0.1}Mn_{1.9}O_4$ increases the exchange current density and facilitates the charge transfer reaction of the active material. The $mCrO_{2.65}$ precursor in $LiCr_{0.1}Mn_{1.9}O_4$ forms a passive film which has lower resistance than the film formed on pure spinel. Potentiostatic experiments carried out to determine the cumulative capacity loss of pure spinel, and $mCrO_{2.65}$ doped indicated that the $mCrO_{2.65}$ doped spinel showed the lowest capacity loss.

5. List of symbols

a	lattice constant, Å
B	Warburg coefficient, $\Omega\ s^{-1/2}$
c	concentration of the electrolyte in the liquid phase, mol cm^{-3}
c_s	concentration of lithium ions in the solid phase, mol cm^{-3}
c_t	concentration of total sites in the solid host material, mol cm^{-3}
C_{dl}	double layer capacitance, μF
C_{sl}	surface layer capacitance, μF

d_{obs}	observed d spacing, Å
d_{cal}	calculated d spacing, Å
D_{Li^+}	diffusion coefficient of Li ion in cathode, m^2 s^{-1}
E	open circuit potential, V
F	Faradaic constant, 96 487 C eq^{-1}
i_0	exchange current density, A g^{-1}
i	current per unit mass, A g^{-1}
k	rate constant
L	finite length of diffusion, cm
n	number of electrons
R	gas constant, 8.314 J mol^{-1} K^{-1}
R_s	electrolyte resistance, Ω
R_{sl}	surface layer resistance, Ω g
S	area, m^2
T	temperature, K
u	oxygen positional parameter
V_m	molar volume, cm^3
x	stoichiometric coefficient for positive electrode, $Li_xCr_yMn_{2-y}O_4$
y	dopant (Cr) concentration
Z	impedance, Ω
Z_W	Warburg impedance, Ω

Greek symbols

β	symmetry factor, dimensionless
η	overpotential, V
ε	permittivity, F m^{-1}
ω	angular frequency, Hz

Acknowledgements

The authors gratefully acknowledge the financial support provided by DOE Division of Chemical Sciences, Office of Basic Sciences, G.M. DE-FG02-96ER 14598 and by Office of Research and Development C/O No. 93-FI48100-100.

References

[1] J.C. Hunter, J. Solid State Chem. 39 (1981) 142.
[2] M.M. Thackeray, W.I.F. David, P.G. Bruce, J.B. Goodenough, Mat. Res. Bull. 18 (1983) 461.
[3] T. Ohzuku, M. Kitagawa, T. Hirai, J. Electrochem. Soc. 137 (1990) 769.
[4] J.M. Tarascon, E. Wang, F.K. Schkoohi, W.R. McKinnon, S. Colson, J. Electrochem. Soc. 138 (1991) 2859.
[5] M. Hosoya, H. Ikuta, T. Uchida, M. Wakihara, J. Electrochem. Soc. 144 (1997) L52.
[6] T. Nagaura, K. Tozawa, Progress in Batteries and Solar Cells 9 (1991) 209.
[7] J.M. Tarascon, D. Guyomard, J. Electrochem. Soc. 138 (1991) 2864.
[8] D. Guyomard, J.M. Tarascon, J. Electrochem. Soc. 139 (1992) 937.
[9] F.K. Shokoohi, J.M. Tarascon, B.J. Wilkens, D. Guyomard, C.C. Chang, J. Electrochem. Soc. 139 (1992) 1845.
[10] D. Guyomard, J.M. Tarascon, J. Electrochem. Soc. 140 (1993) 3071.
[11] J.M. Tarascon, D. Guyomard, Electrochim. Acta 38 (1993) 1221.
[12] J.M. Tarascon, W.R. McKinnon, F. Coowar, T.N. Bowmer, G. Amatucci, D. Guyomard, J. Electrochem. Soc. 141 (1994) 1421.
[13] Y. Gao, J.R. Dahn, J. Electrochem. Soc. 143 (1996) 100.
[14] Y. Gao, J.R. Dahn, J. Electrochem. Soc. 143 (1996) 1783.
[15] Y. Gao, M.N. Richard, J.R. Dahn, J. Appl. Phys. 80 (1996) 4141.
[16] D.H. Jang, J.Y. Shin, S.M. Oh, J. Electrochem. Soc. 143 (1996) 2204.
[17] R.J. Gummow, A. de Kock, M.M. Thackery, Solid State Ionics 69 (1994) 59.
[18] A. Yamada, J. Solid State Chem. 122 (1996) 160.
[19] L. Guohua, H. Ikuta, T. Uchida, M. Wakihara, J. Electrochem. Soc. 143 (1996) 178.
[20] A. Sigala, D. Guyomard, A. Verbaere, Y. Piffard, M. Tournoux, Solid State Ionics 81 (1995) 167.
[21] P. Arora, B.N. Popov, R.E. White, J. Electrochem. Soc. 145 (1998) 807.
[22] W. Baochen, X. Yongyao, F. Li, Z. Dongjinag, J. Power Sources 43–44 (1993) 539.
[23] A.D. Robertson, S.H. Lu, W.F. Averil, W.F. Howard, J. Electrochem. Soc. 144 (1997) 3500.
[24] A.D. Robertson, S.H. Lu, W.F. Howard, J. Electrochem. Soc. 144 (1997) 3505.
[25] P. Arora, G. Zheng, B.N. Popov, R.E. White, The Electrochemical Society Meeting Extended Abstracts, Vol. 97-1, Abstract No. 90, Montreal, Canada, The ECS, Pennington, NJ, May 3–9, 1997, p. 104.
[26] A. Mosbach, A. Verbaere, M. Tournaoux, Mater. Res. Bull. 18 (1983) 1375.
[27] M.M. Thackeray, P.J. Johnson, L.A. de Picciotto, P.G. Bruce, J.B. Goodenough, Mater. Res. Bull. 19 (1984) 179.
[28] W.I.F. David, M.M. Thackeray, P.G. Bruce, J.B. Goodenough, Mater. Res. Bull. 19 (1984) 99.
[29] G. Pistoia, G. Wang, C. Wang, S. S. Ionics 58 (1992) 285.
[30] A.R. West, Solid State Chemistry and Its Application, Wiley, New York, 1987.
[31] M. Castellanos, A.R. West, J. Chem. Soc. Faraday 76 (1980) 2159.
[32] A.R. West, F.P. Glasser, J. Materials Sci. 5 (1970) 676.
[33] M.A. Tena, E. Cordoncillo, G. Monros, J. Carda, P. Escribano, Mater. Res. Bull. 30 (1995) 933.
[34] G. Greatrex, N.N. Greenwood, M. Lal, Mater. Res. Bull. 15 (1980) 113.
[35] Y. Shimony, L. Ben-Dor, Mater. Res. Bull. 15 (1980) 227.
[36] W. Borchardt-Ott, Crystallography, Springer, New York, 1993.
[37] G. Zheng, B.N. Popov, R.E. White, J. Electrochem. Soc. 143 (1996) 435.
[38] G. Zheng, B.N. Popov, R.E. White, J. Electrochem. Soc. 143 (1996) 834.
[39] T.F. Fuller, M. Doyle, J. Newman, J. Electrochem. Soc. 141 (1994) 1.
[40] H. Kanoh, Q. Feng, T. Hirotsu, K. Ooi, J. Electrochem. Soc. 143 (1996) 2610.
[41] M.G. Thomas, P.G. Bruce, J.B. Goodenough, J. Electrochem. Soc. 132 (1985) 1522.
[42] S.-I. Pyun, J.-S. Bae, Electrochim. Acta 41 (1996) 919.
[43] G. Pistoia, A. Antonini, R. Rosati, D. Zane, Electrochim. Acta 41 (1996) 2683.